Acta Astronautica 128 (2016) 119–130

Contents lists available at ScienceDirect

Acta Astronautica

journal homepage: www.elsevier.com/locate/aa

Hybrid rocket propulsion systems for outer planet exploration missions ☆

Elizabeth T. Jens *, Brian J. Cantwell, G. Scott Hubbard

Stanford University, United States

ARTICLE INFO

Article history:
Received 29 February 2016
Received in revised form
16 June 2016
Accepted 19 June 2016
Available online 22 June 2016

ABSTRACT

Outer planet exploration missions require significant propulsive capability, particularly to achieve orbit insertion. Missions to explore the moons of outer planets place even more demanding requirements on propulsion systems, since they involve multiple large ΔV maneuvers. Hybrid rockets present a favorable alternative to conventional propulsion systems for many of these missions. They typically enjoy higher specific impulse than solids, can be throttled, stopped/restarted, and have more flexibility in their packaging configuration. Hybrids are more compact and easier to throttle than liquids and have similar performance levels. In order to investigate the suitability of these propulsion systems for exploration missions, this paper presents novel hybrid motor designs for two interplanetary missions. Hybrid propulsion systems for missions to Europa and Uranus are presented and compared to conventional in-space propulsion systems. The hybrid motor design for each of these missions is optimized across a range of parameters, including propellant selection, O/F ratio, nozzle area ratio, and chamber pressure. Details of the design process are described in order to provide guidance for researchers wishing to evaluate hybrid rocket motor designs for other missions and applications.

1. Introduction

Hybrid rocket motors are a form of chemical propulsion system where the fuel and oxidizer are stored in different phases. The typical hybrid motor configuration uses a solid fuel grain and a liquid or gaseous oxidizer. The fuel is contained within the combustion chamber in the form of a cylinder, with one or more channels called ports hollowed out along its axis. The oxidizer is delivered to the combustion chamber through a single fluid feed system. A main run valve is used to control this delivery. An igniter is used to vaporize some of the fuel and initiate combustion. Combustion takes place within a turbulent boundary layer through diffusive mixing between oxidizer flowing through the port and fuel melting/pyrolizing and evaporating from the solid surface. Once a diffusion flame is established over the fuel surface the process is self-sustaining. The regression rate of the fuel, and hence the rate of burning, is dependent upon the mass flux within the combustion chamber. However, the regression rate is independent of the chamber pressure over most of the oxidizer flux range, allowing the chamber pressure to be a free variable in the chamber design. Throttling can be achieved simply by limiting the rate of oxidizer delivery to the combustion chamber.

Hybrid rocket motors are throttle-able, able to be stopped and restarted and use energetic propellant combinations to deliver relatively high specific impulse, greater than solid rocket motors and monopropellant thrusters, comparable to bi-propellant liquid engines. Hybrid motors are mechanically simpler than liquid engines as they only require one liquid feed system and are also typically more compact than liquid systems, due to the higher density of their propellants. Hybrid motors benefit from flexibility in their packaging configuration. Hybrid motors are much safer than both solid and liquid systems as the fuel and oxidizer are separated physically by phase, making it difficult to achieve an intimate mixture of a large amount of propellant even in the event of an engine failure. Hybrid motor fuels are also inert hydrocarbons that are non-toxic. Hybrid motors have potential cost benefits over existing liquid and solid systems. These potential advantages make hybrid rocket motors promising candidates for in-space propulsion.

In recent years there has been increasing interest in using hybrid rocket motors for interplanetary missions [1,2]. Preliminary design studies have shown hybrid motors to be viable alternatives to conventional propulsion systems for some exploration missions [3–6]. Reference [3] and Reference [5] investigated utilizing hybrid motor technology for a Mars Ascent Vehicle (MAV). According to the analysis presented in Reference [3] a hybrid MAV could have a

☆Original version presented at the 66th International Astronautical Congress, Jerusalem, Israel as paper IAC-15-C4.6.10.

* Corresponding author.
E-mail addresses: bethjens@gmail.com (E.T. Jens), cantwell@stanford.edu (B.J. Cantwell), scotthub@stanford.edu (G.S. Hubbard).

http://dx.doi.org/10.1016/j.actaastro.2016.06.036
0094-5765/

mass saving of up to 79 kg, representing a 22% total system wet mass saving, compared to the baseline solid propulsion system. Reference [4] investigated using a hybrid propulsion system for a main in-space propulsion motor and found that the hybrid propulsion system could have a significant propellant mass saving over the baseline liquid system. Reference [6] investigated a small-scale hybrid propulsion system for a Mars aerocapture demonstration mission, and also found the hybrid propulsion system to be a viable alternative to the baseline monopropellant hydrazine system.

This paper extends the analysis of Reference [4] by applying the more rigorous design approach adopted in Reference [6] to exploration missions requiring significant in-space propulsive capabilities.

2. Mission selection

This paper presents novel hybrid motor designs for two interplanetary missions which each require large propulsive maneuvers for orbit insertion. The two destinations of interest are Europa and Uranus. These destinations were selected in line with the recommendations of the Decadal Survey [7] based on their level of scientific interest and the programmatic likelihood of a mission in approximately the next 20 years.

Europa has been described as “one of the most important targets in all of planetary science” due to the potential for life to exist in its ocean [7]. Interest in the habitability of Europa has led to the development of the Europa Clipper mission concept, which recently passed initial review and entered the formulation phase [8]. The baseline propulsion system for this flyby mission is based on the version of the propulsion system presented in the 2012 review of this concept [9]. This propulsion system was required to provide 1.52 km/s ΔV for maneuvers, Thrust Vector Control (TVC) during the main engine burns, the Attitude Control System (ACS) for times when reaction wheels are not being used, and reaction wheel unloading. The system was also designed to provide radiation shielding for avionics components. The baseline design uses a dual-mode hydrazine (N_2H_4) and nitrogen tetroxide (NTO) bi-propellant system. This propulsion system is designed with one main motor, four TVC thrusters, and sixteen ACS thrusters. The main bi-propellant engine has a thrust of 458 N. Hydrazine monopropellant thrusters with 22 N and 4.4 N of thrust are used for TVC and ACS, respectively. The propellant budget for this baseline propulsion system is provided in Table 1.

Uranus was selected as the second target of interest to be examined in this paper. Uranus is an ice giant, “the only class of planet that has never been explored in detail,” Reference [7]. A Uranus Orbiter and Probe mission was selected as the third-highest-priority flagship mission in the Decadel Survey [7] and hence it is of interest to examine a hybrid propulsion system for such a mission. The reference mission for this destination planet is taken from Reference [10]. This mission design uses a propulsion system very similar to that described for the Europa flyby mission. The requirements are to have a propulsion system capable of providing 1.958 km/s ΔV for maneuvers, TVC during the main engine burns, ACS for times when reaction wheels are not being used, and reaction wheel unloading. The propellant is again hydrazine and nitrogen tetroxide. The single main bipropellant engine has 645 N of thrust, the four monopropellant thrusters for TVC each have 22 N of thrust, and the eight monopropellant thrusters for ACS each have 1 N of thrust. The propellant masses for the Uranus reference mission are detailed in Table 2.

Table 1
Propellant budget for baseline Europa Flyby mission concept [9]. Note that MR refers to the Mixture Ratio.

Required Propellant	Mass [kg]
Propellant for 1.52 km/s ΔV	
Hydrazine (MR=0.85)	465
NTO	395
Total	860
Hydrazine for TVC	75
Hydrazine for ACS	40
Hydrazine Residual (2.5%)	14
NTO Residual (2.5%)	10
Total Hydrazine	594
Total NTO	405
Pressurant Gas	6
Total Propellant	1005

Table 2
Propellant budget for baseline Uranus mission [10]. Note that MR refers to the Mixture Ratio.

Required Propellant	Mass [kg]
Propellant for 1.96 km/s ΔV	
Hydrazine (MR=0.85)	758
NTO	644
Total	1403
Hydrazine for TVC and ACS	136
Hydrazine Residual (2.5%)	23
NTO Residual (2.5%)	17
Total Hydrazine	917
Total NTO	661
Pressurant Gas	7
Total Propellant	1585

3. System requirements

The system requirements for the hybrid propulsion systems designed in this paper are taken from the propulsion system requirements for the two reference mission architectures discussed in the previous section. Specifically, each hybrid propulsion system is required to provide propulsion for large maneuvers, with the capability to provide the total ΔV shown in Table 3, TVC during main engine operation, ACS in the event that reaction wheels are not being used, and reaction wheel unloading.

The interplanetary nature of the two missions, with long multi-year cruise phases, see Table 3, necessitates the consideration of only storable or high-pressure gas oxidizer options. Thus, the use of cryogenic oxidizers, such as liquid oxygen, is precluded from consideration. The system is designed for nominal operation at 20 °C.

The thrust of the propulsion system must be such that the maximum acceleration of the spacecraft is always less than 3 g (29.4 m/s^2) if the spacecraft uses Radioisotope Thermoelectric

Table 3
Summary of key mission parameters for two reference missions. Values from References [9–11].

Parameter	Units	Europa	Uranus
ΔV	[km/s]	1.52	1.96
Spacecraft Wet Mass*	[kg]	2354	3345
Cruise Phase	[years]	6.37	14

* Spacecraft mass for the Europa reference mission is Current Best Estimate (CBE) mass. Spacecraft mass for the Uranus reference mission is maximum launch capability. These different definitions were selected in order to be consistent with the values used for propulsion system trades in each reference mission.

Generators (RTGs) as its source of power, and less than 1 g (9.8 m/s^2) if the spacecraft uses solar arrays.

Heritage components are used wherever possible in order to mitigate risk associated with adopting a novel propulsion system over the proven dual mode bi-propellant baseline systems.

4. Design methodology

A simplified overview of the design process adopted to calculate all primary propulsion system masses presented in this paper is shown schematically in Fig. 1. Current literature on hybrid rocket system design, References [3–6], does not describe the methodology used to generate the final hybrid rocket motor design. This detail is provided here in order to both provide guidance for researchers wishing to evaluate hybrid rocket motor designs for other missions and applications, and to elucidate some of the challenges involved with designing these systems given the current Technology Readiness Level (TRL) of hybrid rocket motor technology and the limited availability of test data for these systems.

As described in the previous section, this paper evaluates hybrid rocket motor designs for two missions with baseline liquid propulsion systems. The required ΔV for each mission is taken from the baseline mission and is the main requirement for the propulsion system. The baseline design masses and payload masses are used to give an indication of the total mass of the system to be analysed. If the mass of the hybrid propulsion system is larger

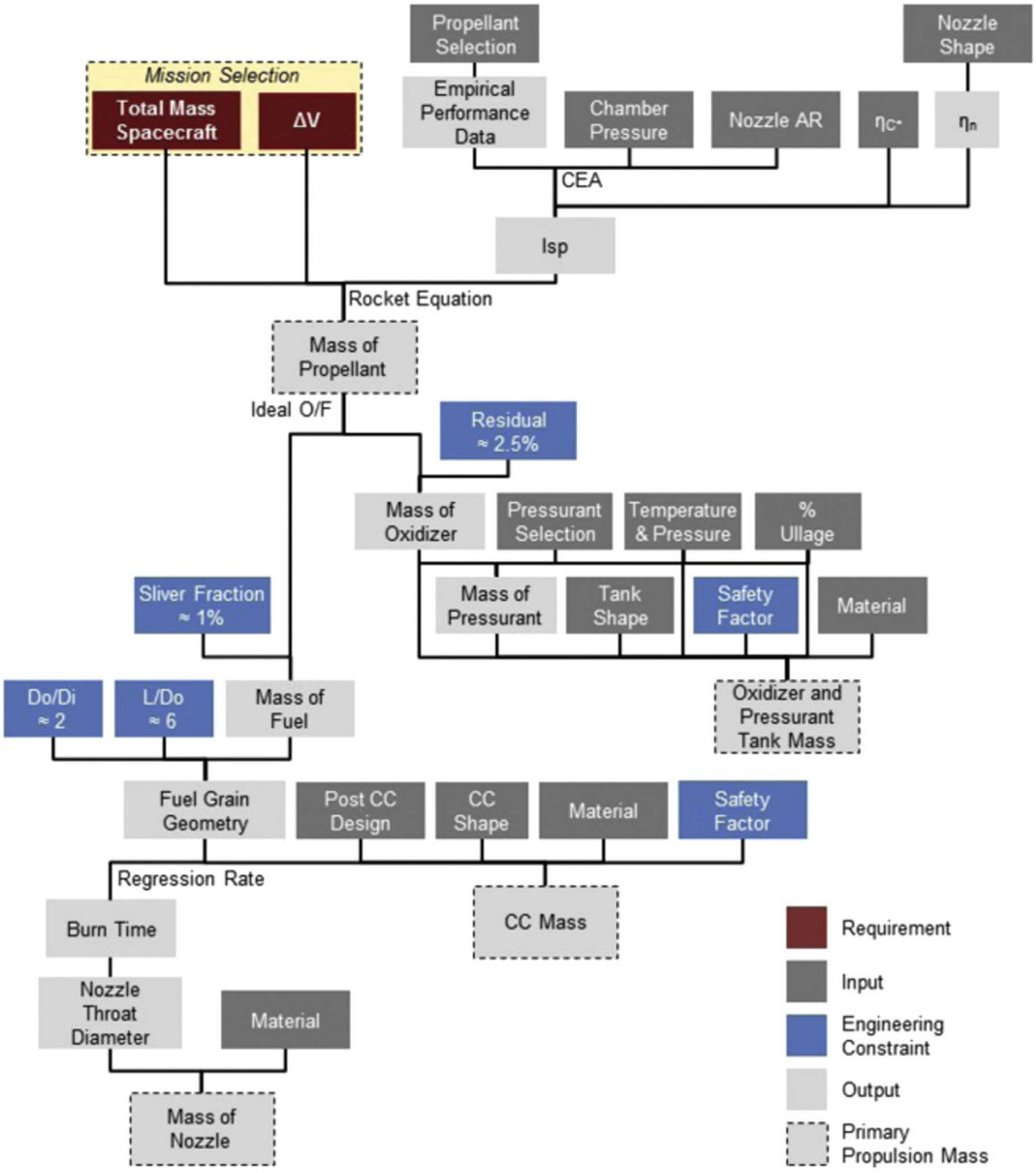

Fig. 1. Simplified overview of the hybrid rocket motor design process adopted in this paper. Details of each step and pertinent equations are provided in the text. AR refers to Area Ratio. η_{c^*} and η_n are the combustion and nozzle efficiency, respectively. CEA refers to Chemical Equilibrium with Applications, see Reference [12]. *O/F* is the ratio of oxidizer to fuel mass. D_O and D_i refer to the outer and inner fuel grain diameter, respectively. *L* refers to the fuel grain length. CC refers to Combustion Chamber.

Table 4
Summary of oxidizer properties. Data is taken from References [13–17].

Oxidizer Name	Chemical Composition	Density at 298 K [kg/m^3]	Freezing Temperature [K]††	Boiling Temperature [K]††
MON-3	97% N2O4 + 3% NO	1.433×10^3	261.95	294.4
Nitrogen Tetroxide	N_2O_4 or N_2O_4 +1% NO	$1.433 \times 10^{3*}$	261.95	294.4
IRFNA	82-85% HNO_3 + 13–15% N_2O_4 + 2–3% H_2O + 0.4-0.6% HF	$1.583 \times 10^{3*}$	221.15	337.3 - 373.2
Nitrous Oxide	N_2O	776**	182.3	184.7
Hydrogen Peroxide	H_2O_2	1.414×10^3	272.72	423.4
Gaseous Oxygen	O_2	1.331†	54.36	90.2

* Liquid density at pressures above vapor pressure.
** Saturated liquid density at a pressure of 6895 kPa (1000 psi).
† The density of gaseous oxygen is shown for storage at 293.15 K and 101.3 kPa.
†† Temperatures listed for storage at atmospheric pressure.

or smaller than the mass of the baseline propulsion system then this is interpreted as a net decrease or increase, respectively, of the available payload mass as compared to the baseline design. This approach removes the need for iterative design as would be required if the payload mass were held constant and the propulsion system mass adjusted to achieve the required ΔV for a spacecraft with a larger or smaller total mass. Thus, in this paper the total system wet mass is treated as a requirement for the propulsion system design.

The nature of the mission being analysed places further requirements on the propulsion system, particularly in regard to propellant selection. As described in the previous section, the long timeline associated with interplanetary missions restricts the choice of oxidizer to include only storable and gaseous oxidizers. The selection of fuel remains relatively unaffected.

The potential oxidizers for an in-space hybrid propulsion system are listed along with their properties in Table 4. The oxidizers presented are MON-3 (N_2O_4, +3% NO, by mass), nitrogen tetroxide (N_2O_4), Inhibited Red-Fuming Nitric Acid (IRFNA) (82-85% HNO_3 + 13–15% N_2O_4 +2–3% H_2O + 0.4–0.6% HF, by mass), nitrous oxide (N_2O), hydrogen peroxide (H_2O_2), and gaseous oxygen (O_2). The oxidizer selected for a given mission is typically chosen for its performance, density, suitability for long-term storage, and flight heritage.

All hybrid rocket fuels considered in this paper are inert hydrocarbons, however they differ widely in their appearance, structural properties, performance and burn rate. Five different solid hydrocarbon fuels are considered; namely paraffin wax, PolyEthylene (PE) wax, Hydroxyl-Terminated PolyButadiene (HTPB), High Density PolyEtheylene (HDPE), and Poly-Methyl MethAcrylate (PMMA) fuel grains are investigated. These five fuel grains were chosen as they span a range of burn rates and there is published regression rate data for the combustion of these fuels with some oxidizers. The first two fuels, paraffin wax and PE wax, are liquefying high regression rate fuels, whilst the last three fuels, HTPB, HDPE and PMMA are classical hybrid rocket fuels. The thermochemical properties assumed for these fuels are provided in Table 5. There are other candidate fuel grain materials such as nylon and Acrylonitrile Butadiene Styrene (ABS) that are not discussed here.

Table 5
Summary of hybrid rocket fuel properties. Data is taken from References [18–21].

Name [-]	Molecular Formula [-]	Heat of Formation [kcal/mol]	Density [kg/m^3]
Paraffin	$C_{32}H_{66}$	−224	925
PE Wax	$[C_2H_4]_n$	−13	940
HTPB	$C_{654}H_{988}N_8O_{20}$	1142	919
HDPE	$[C_2H_4]_n$	−13	960
PMMA	$[C_5H_8O_2]_n$	−103	1180

The performance and properties of hybrid rocket fuels can be altered to some extent through the addition of solid additives, such as metals and metal hydrides. The use of micron sized aluminum additives is considered here as a means to increase the specific impulse and density impulse of the motor. The addition of aluminum particles also has the effect of adjusting the ideal oxidizer to fuel mass ratio (O/F) of the motor.

A fuel and oxidizer combination that satisfies requirements for storability, safety, system heritage, and potentially also requirements for compatibility is chosen. In order to evaluate the performance of this fuel and oxidizer the chamber pressure and nozzle Area Ratio (AR) must first be selected. These values, along with the thermochemical properties of the propellants, see Tables 4 and 5, are inputs to a chemical equilibrium solver, which determines the final composition of the mixture after combustion by finding the composition that minimizes the Gibbs free energy of the mixture. In this work Chemical Equilibrium with Applications (CEA), see Reference [12], is used to perform all such calculations and determine the ideal specific impulse, Isp_{ideal}, of the propellant combination. Note that the ideal specific impulse is optimized across a range of oxidizer to fuel mass ratios (O/F) for the propellant combination. The O/F corresponding to the maximum ideal specific impulse is used for the remainder of the design. There can be instances where non-ideal O/F ratios are desirable, such as when volume constraints outweigh performance benefits, but in general the selection of O/F resulting in maximum specific impulse optimizes the total mass of the final design [22].

The ideal specific impulse is multiplied by the combustion efficiency and nozzle efficiency in order to generate a more realistic prediction of the delivered Isp of the propulsion system. A c* efficiency of 95% is assumed throughout this paper, consistent with the achieved ground test results of Reference [23]. The shape of the nozzle determines the nozzle efficiency; a nozzle efficiency of 98% is assumed for a conical nozzle and 99% for a bell shaped nozzle. These values are taken from Reference [14].

The total spacecraft mass, required ΔV, and the specific impulse of the propellants are then input to the rocket equation, Eq. 1, to determine the total propellant mass required.

$$m_{prop} = m_{total}\left[1 - e^{\left(\frac{-\Delta v}{Isp\, g}\right)}\right] \quad (1)$$

Here m_{prop} is the propellant mass, m_{total} is the total spacecraft wet mass, Isp is the ideal specific impulse of the motor multiplied by the c^* and nozzle efficiencies, and g is 9.8 m/s^2. This propellant mass is then separated into the oxidizer mass and fuel mass using the ideal O/F ratio. A 2.5% residual oxidizer mass is assumed. An oxidizer tank ullage of 5% is also assumed for all liquid oxidizers.

If an external pressurant is used, then the required pressurant mass is calculated assuming that all of the liquid oxidizer is expelled from the tank and the pressurant is used to maintain a

constant oxidizer tank pressure throughout the burn. The expansion of the pressurant gas is assumed to be isothermal. This assumption is equivalent to assuming that the heat transfer from heaters and avionics is sufficient to overcome cooling associated with pressurant gas expansion and therefore to maintain constant temperature in the tanks. This scenario would occur if the oxidizer were expelled over a long time scale. An alternative approach would be to assume that the oxidizer is expelled over a very short time period; precluding significant external heating of the tank during the burn. This is equivalent to assuming that the pressurant gas expands adiabatically. The adiabatic and isothermal assumptions bound the range of possible tank conditions. Following the calculation of the required pressurant mass along with the corresponding volumes of the oxidizer and pressurant tanks, the mass of these tanks is then determined.

The oxidizer and pressurant tanks are defined to be either metallic tanks or Composite Overwrapped Pressure Vessels (COPVs). The mass of the COPV tanks is calculated using an empirical scaling law. The COPV tanks use a metallic liner assumed to be 0.762 mm (0.03 in.) thick. The material of this liner is selected based on material compatibility with the oxidizer and pressurant. The metallic tanks are constructed of a material compatible with the oxidizer and pressurant and do not require an additional liner.

The metallic oxidizer and pressurant tank masses are calculated using structural calculations for a thin-walled pressure vessel. Spherical and cylindrical tanks with hemispherical end caps are investigated; the wall thickness, t_{sphere} and t_{cyl}, is determined from Eqs. 2 and 3, respectively. A safety factor, k, of 1.5 is used for all structural calculations. If the required thickness of the tanks is calculated to be less than the minimum material thickness for machinability then the tank thickness is set to this minimum material thickness, which is defined to be 0.762 mm (0.03 in.) for all structures presented in this paper.

$$t_{\text{sphere}} = \frac{kPr_{\text{sphere}}}{2\sigma_y} \tag{2}$$

$$t_{\text{cyl}} = \frac{kPr_{\text{cyl}}}{\sigma_y} \tag{3}$$

Where σ_y is the yield stress of the tank material, P is the Maximum Expected Operating Pressure (MEOP) of the tank, and r is the tank radius. The mass of the metallic oxidizer and pressurant tanks is then able to be determined based on the density of the selected materials, along with the external geometry and thickness of the tanks.

The total mass of the fuel grain is increased to account for the unburned sliver fraction. A sliver fraction of 1% is assumed as this value has been achieved during hybrid rocket ground testing. It is assumed that the fuel grain is cylindrical and has a single port. Structural considerations for a thick-walled cylinder dictate that the ratio of the outer diameter, D_o, to the inner diameter, D_i, of the fuel grain should be around 2. This is of particular importance for high regression rate fuels, such as paraffin and PE wax, which are brittle materials with comparably lower tensile strengths. A fuel grain length-to-diameter ratio of around 6 is initially also used. This value is used in order to provide sufficient length for mixing, leading to adequate propellant utilization, and to ensure operation over a reasonable range of mass fluxes, G, in the port. The range of mass fluxes for a given design is checked at the end of the design cycle. The length to diameter ratio of the fuel grain is not required to be exactly 6, this is simply a rule of thumb and can be increased or decreased as needed in order to improve the final design of the motor in terms of the burn time, the operating range of mass fluxes, and the packaging configuration. The fuel grain geometry is thus determined from the total mass of fuel and these engineering constraints on the length and diameter ratios. An insulator is selected, typically garolite or paper phenolic; a garolite $G10$ liner with 0.5 mm (0.0197 in.) thickness is assumed for these designs. The mass of this liner is calculated and included with the combustion chamber mass. The thickness of the combustion chamber wall is calculated using Eq. 3 assuming that the combustion chamber is made of titanium and is a thin walled pressure vessel. The geometry of the pre and post combustion chamber is input and the total mass of the combustion chamber is calculated.

As can be seen in Fig. 1, the next step in the design process is to determine the burn time. This is the time that it takes to burn the full fuel grain and oxidizer. This is not a free variable in the design with the current formulation, as the burn rate of the fuel is a function of the fuel grain geometry and oxidizer mass flux, which is already fixed if one is to achieve the ideal O/F. At a given axial position x along the port, the fuel mass transfer rate is proportional to the mass flux averaged across the port, this relationship is known as the regression rate law for a hybrid rocket, see Eq. 4.

$$\dot{r} = ax^{-m}G^n \tag{4}$$

$$\text{where } G = \frac{\dot{m}_o + \dot{m}_f}{\pi r^2} = \frac{\dot{m}_{\text{port}}}{\pi r^2} \tag{5}$$

G is the mass flux in the port, r is the radius of the port, and $\dot{m}_o$ and $\dot{m}_f$ are the oxidizer and fuel mass flow rates, respectively. The constants and a, n and m are empirically determined parameters for a given fuel/oxidizer combination. The fuel mass flow rate, $\dot{m}_f$, increases with axial distance along the port leading to coupling between the local fuel regression rate and the local mass flux. Because axial regression rate dependence is small, the effect of the length dependence on the regression is often neglected. Furthermore, it can be shown that the regression rate behavior can be written solely in terms of oxidizer mass flux, as:

$$\dot{r} = a_o G_o{}^n \tag{6}$$

Here G_o is the average oxidizer mass flux. Eq. 6 is used to design hybrid rocket motors for all of the initial trades presented in this paper. The use of Eq. 6 to design a hybrid rocket motor is commonly adopted [3–6], however it can lead to inaccuracies in the design, particularly with regard to the achieved O/F ratio [6].

With current formulation using Eq. 6 and the assumption of regulated oxidizer mass flow rate, the burn time can be written:

$$t_{burn} = \left[\frac{\left(D_f^{2n+1} - D_i^{2n+1}\right)\pi^n}{a_o(2n+1)M_{ox}^n} \right]^{\frac{1}{1-n}} \tag{7}$$

Here t_{burn} is the burn time, D_i and D_f are the initial and final port diameter respectively, and M_{OX} is the total mass of oxidizer. This expression for burn time is very sensitive to the selection of the empirical regression rate constants a_o and n. There is much scatter and disagreement in referenced data for these constants and hence the burn time calculated using this method must be treated as indicative only and confirmed by testing. The disagreement in the data likely stems from the dependence of a_o on the O/F ratio. Unfortunately, it is not common practice to publish the oxidizer to fuel ratio at which a given value of a_o and n was determined.

It is of interest to see how sensitive the regression rate is to small changes in the parameters a, n, and m. Let the parameters be changed by small amounts.

$$a \rightarrow aa'$$

$$n \rightarrow n + n'$$

$m \rightarrow m + m'$

The regression rate equation, Eq. 4, becomes

$$\frac{\partial r}{\partial t} = \frac{aa'}{x^{m+m'}}\left(\frac{\dot{m}_{port}}{\pi r^2}\right)^{n+n'} \tag{8}$$

The ratio of the perturbed to unperturbed regression rate for constant oxidizer mass flow rate is

$$\frac{\frac{\partial R}{\partial \tau}}{\frac{\partial R}{\partial \tau}\Big|_{(n',m')=(0,0)}} = \left(\frac{a'\pi^{n'}}{r(0,0)^{m'}}\left(\frac{\dot{m}_{ox}(0)}{\pi r(0,0)^2}\right)^{n'}\right)\frac{1}{\chi^{m'}}\left(\frac{J}{\pi r^2}\right)^{n'} \tag{9}$$

where

$$R = \frac{r(x,t)}{r(0,0)}$$

$$\tau = \frac{t}{t_{burn}}$$

$$J = \frac{\dot{m}_{ox} + \dot{m}_f(x,t)}{\dot{m}_{ox}}$$

$$\chi = \frac{x}{r(0,0)}$$

Note that the relative error in the regression rate is the same as the relative error in the fuel mass flow rate. For small changes in n and m, and values of a' very close to one we can approximate Eq. 9 as

$$\frac{\frac{\partial R}{\partial \tau}}{\frac{\partial R}{\partial \tau}\Big|_{(n',m')=(0,0)}} \cong 1 + n'\left\{ln\left(\frac{(a')^{\frac{1}{n'}}\pi}{r(0,0)^{\frac{m'}{n'}}}\left(\frac{\dot{m}_{ox}(0)}{\pi r(0,0)^2}\right)\right) + ln\left(\frac{J}{(\chi)^{\frac{m'}{n'}}\pi r^2}\right)\right\} \tag{10}$$

The first term multiplying n' in Eq. 10 is a fixed number and, to a good approximation, is the logarithm of π times the initial flux in the port, typically a number in the range 5 to 8. The second term in brackets is approximately the logarithm of the dimensionless flux in the port and depends on space and time. The dimensionless flux is generally less than one so this factor tends to be negative except near the port entrance. For m = 0 the second factor is approximately -ln(1/π)=1.14. Thus, in general, small changes in n change the rates substantially more than comparable changes in a or m, see Eq. 11, and therefore have a correspondingly larger effect on the system design.

$$\frac{\frac{\partial R}{\partial \tau}}{\frac{\partial R}{\partial \tau}\Big|_{(n',m')=(0,0)}} \cong 1 + \sim 7n' \tag{11}$$

The disagreement in the regression rate parameters a_o and n can most clearly be seen by looking at test results for the combustion of HTPB with oxygen. Table 6 lists published values of a_o and n, the corresponding prediction of regression rate using these values is shown in Fig. 2. The values of a_o for regression rates in m/s and mass flux in kg/m^{2}s range between 2.85×10^{-5} and 8.75×10^{-5}, representing a variation of up to 3 times the published value. Values for n range between 0.53 and 0.68. The lack of agreement on the empirical parameters is particularly pronounced for the combustion of HTPB, likely due to differences in the fuel formulation resulting from variation in the curing process adopted by each group of researchers. However, the inconsistency in the published values still exists to some degree for other fuel and oxidizer combinations, due to the dependence of a_o on the O/F. Hence, the burn rates and motor designs presented in this and other design papers should be treated as indicative only; a full test campaign is always recommended to validate a motor design.

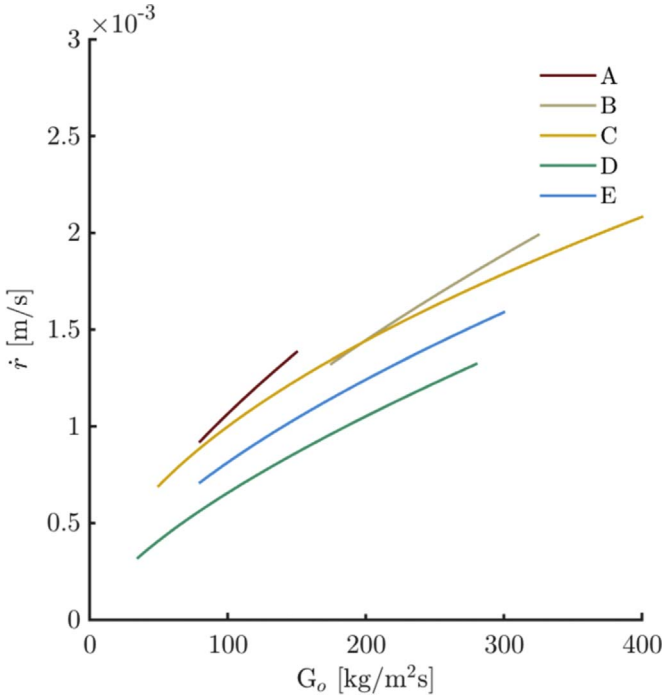

Fig. 2. Regression rate versus oxidizer mass flux of HTPB fuel combusting with O_2 according to Eq. 6. Regression rate law data is provided in Table 6.

The published regression rate parameters used in this paper are shown in Table 7 and Fig. 3.. Test data is not currently published for many of the fuel and oxidizer combinations discussed in this paper. Regression rate parameters are estimated whenever test data is not available. These estimated values of the parameters should be treated as indicative only.

Following the calculation of the burn time using Eq. 7, the operating range of oxidizer mass fluxes should be checked to

Table 6
Regression rate coefficients for the combustion of O_2 with HTPB fuel. Also listed is the range of oxidizer mass flow rates over which these coefficients were determined.

Label	a_o	n	G_o [kg/m^{2}s]	Reference
A	5.41×10^{-5}	0.65	80-150	[24]
B	4.40×10^{-5}	0.66	175-325	[24] Slab
C	8.70×10^{-5}	0.53	50-400	[25]
D	2.85×10^{-5}	0.68	35-280	[15]
E	4.90×10^{-5}	0.61	80-300	[17]

Table 7
Note that the regression rate parameters published for PE wax and IRFNA were not explicitly listed in References [21] and [28]; instead they were calculated using data published in those papers.

Oxidizer	Fuel	a_o	n	Reference
O_2	Paraffin	1.17×10^{-4}	0.62	[26]
O_2	PE Wax	4.31×10^{-5}	0.71	[21]
O_2	HTPB	3.04×10^{-5}	0.68	[26]
O_2	HDPE	2.34×10^{-5}	0.62	[26]
O_2	PMMA	2.11×10^{-5}	0.62	[19]
N_2O	PMMA	1.31×10^{-4}	0.34	[27]
N_2O	HTPB	1.88×10^{-4}	0.35	[27]
N_2O	HDPE	1.16×10^{-4}	0.33	[27]
N_2O	Paraffin	1.55×10^{-4}	0.50	[26]
IRFNA	80% Polybutadiene/ 20% PMMA	3.18×10^{-5}	0.56	[28]

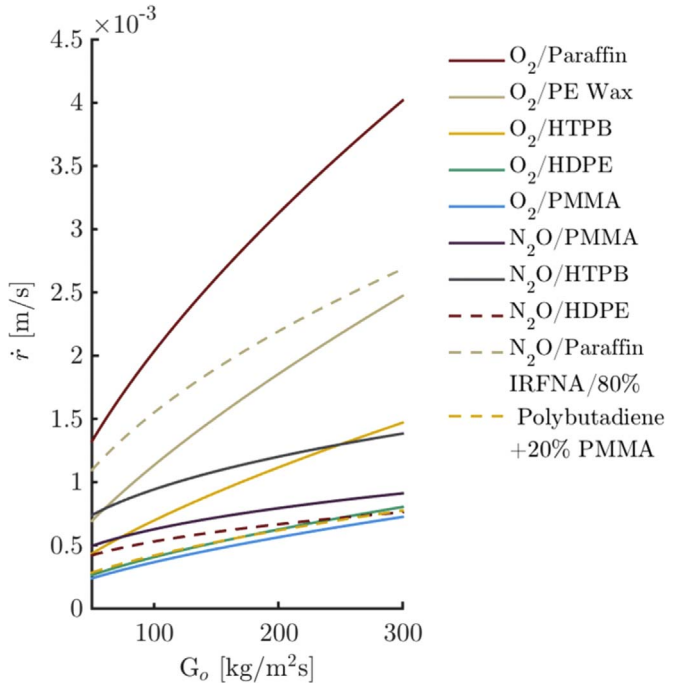

Fig. 3. Regression rate versus oxidizer mass flux for regression rate data provided in Table 7.

ensure that the mass flux is within a normal operating range for hybrid rocket motors throughout the burn. Note that the exact range of reasonable oxidizer mass fluxes is still somewhat up for debate and likely depends on the propellant combination. Some researchers assert that the final mass flux in the motor should be greater than approximately 50 kg/m^{2}s, whilst others report stable motor operation at mass fluxes as low as 0.43 kg/m^{2}s [29]. To be conservative, in this paper we require the oxidizer mass flux to be above 50 kg/m^{2}s for the duration of the motor operation.

The acceleration of the vehicle should also be checked at this point. A maximum acceleration of 3 g (29.4 m/s^2) is imposed for all hybrid rocket motor designs presented in this paper. If the reference missions were to use solar arrays, then a 1 g (9.8 m/s^2) acceleration constraint would be imposed.

If the calculated mass fluxes within the combustion chamber and the vehicle acceleration are reasonable then the design of the motor can be continued, if not then the inputs should be varied in order to generate a more reasonable design.

The nozzle geometry and mass can be determined after the calculation of the burn time. The first step in this process is to determine the size of the nozzle throat using the knowledge that the nozzle throat will be choked and solving for the throat size required to achieve the specified chamber pressure.

The diameter of the nozzle throat must be checked relative to the initial diameter of the fuel port to ensure that the Mach number in the port is low. Given that these motors operate in the vacuum of space; the nozzle throat is guaranteed to be choked. Thus, the upstream Mach number can be estimated using Eq. 12 and the fluid properties of the combustion products output by CEA.

$$\frac{A^*}{A} = \left(\frac{\gamma+1}{2}\right)^{\frac{\gamma+1}{2(\gamma-1)}} \left[\frac{M}{\left(1+\frac{\gamma-1}{2}M^2\right)^{\frac{\gamma+1}{2(\gamma-1)}}}\right] \tag{12}$$

Here A^* refers to the nozzle throat area, A refers to the initial cross-sectional area of the port, γ refers to the ratio of specific heats of the combustion products, and M is the Mach number at the end of the port. This equation neglects the effect of heat addition on the total temperature resulting from combustion between the post combustion chamber and the nozzle throat. A good rule of thumb is to ensure that the Mach number in the port calculated with Eq. 12 is less than approximately 0.3; this corresponds to a diameter ratio, D_i/D_{throat} of at least 1.5.

Assuming that the ratio of port diameter to nozzle throat diameter is reasonable then the nozzle mass can be calculated. The mass of the nozzle is estimated using an empirical equation for solid rocket motor nozzles from Reference [14], with a correction to account for the reduced mass of the hybrid rocket motor nozzle throat insert as compared to a submerged solid rocket motor throat, see Eq. 13.

$$M_{nozzle}=0.256\times10^{-4}\left[\frac{\left(m_{prop}c^*\right)^{1.2}\epsilon^{.3}}{P_c^{0.8}t_{burn}^{0.6}\left(\tan\theta_{cn}\right)^{0.4}}\right]^{0.917} -\left(153D_{throat}+3.3\right) \tag{13}$$

Here M_{nozzle} is the nozzle mass [kg], c^* is the characteristic velocity [m/s], P_c is the combustion chamber pressure [MPa], t_{burn} is the burn time [s], D_{throat} is the nozzle throat diameter [m], ε is the nozzle area ratio, and θ_{cn} is the nozzle half-angle.

The weight of the nozzle, oxidizer tanks, pressurant tanks, and the combustion chamber together constitute the primary structural mass of the propulsion system. This primary propulsion system mass, along with the propellant mass, is used to compare the hybrid motor designs in order to evaluate the various trades. The secondary structures include all feedline valves, fittings and tubing, the igniter, propellant management devices, component supports, and tank mounts and bosses. Cabling associated with the propulsion system is not included in the propulsion system masses. Secondary masses are estimated for the final hybrid motor design in order to compare it to the baseline chemical propulsion system.

5. Results

5.1. Propellant selection

The performance of the oxidizers listed in Table 4 is evaluated by investigating their ideal vacuum specific impulse, Isp_{VAC}, for combustion with neat paraffin wax and with 70% neat paraffin wax and 30% aluminum powder, see Figs. 4 and 5, respectively.

Figs. 4 and 5 show that the performance of gaseous oxygen is superior to the other oxidizers considered in this paper. At the conditions analysed it has a vacuum specific impulse approximately 9% higher than the next best oxidizer, hydrogen peroxide. However, the properties provided in Table 4 show that the density of gaseous oxygen can be three orders of magnitude less than its liquid counterparts. Increasing the pressure at which it is stored can of course increase the density of gaseous oxygen. Fig. 6 shows the density of gaseous oxygen at 293.15 K with increasing pressure. It can be seen that the density can be increased to around 500 kg/m^3 by storing the gas at 41.37 MPa (6000 psi). This increase can reduce the volume required for oxygen enough to make it feasible for some missions [6]. However, a density of 500 kg/m^3 is still only a fraction of the density of the liquid oxidizers and for large systems, the large mass and volume of the high pressure tanks required to store gaseous oxygen outweigh the performance benefit associated with using this oxidizer. Thus, gaseous oxygen is not used in the final system designs presented in this paper.

Hydrogen peroxide is typically listed as a storable oxidizer, and is thus included in Table 4, Figs. 4, and 5, however it is not well-suited to long duration flight missions. Hydrogen peroxide is a

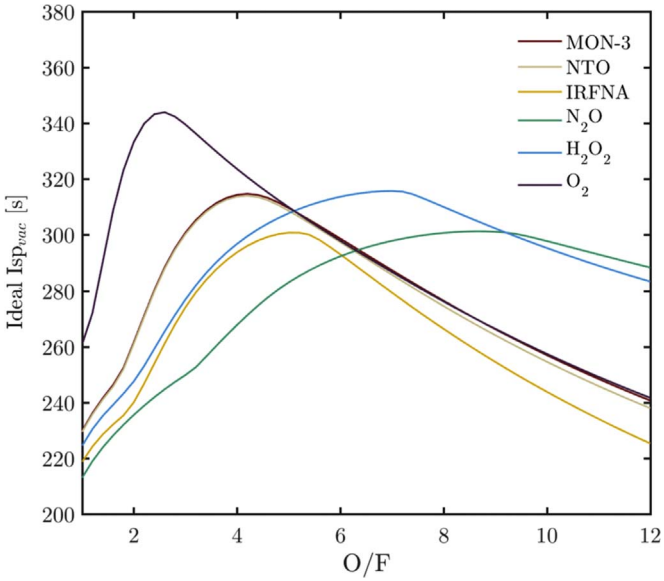

Fig. 4. Ideal Isp_{VAC} versus O/F for a range of oxidizers with paraffin wax. This figure is generated using Chemical Equilibrium with Applications [12], with a nozzle area ratio of 100 and chamber pressure of 1.38 MPa (200 psi).

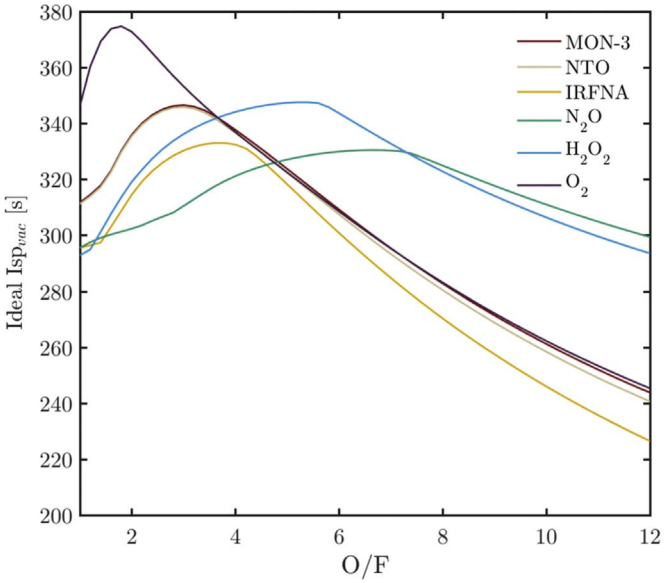

Fig. 5. Ideal Isp_{VAC} versus O/F for a range of oxidizers with 70% paraffin wax and 30% aluminum. This figure is generated using Chemical Equilibrium with Applications [12], with a nozzle area ratio of 100 and chamber pressure of 1.38 MPa (200 psi).

liquid at ambient temperatures [14] and has reasonable performance. However, hydrogen peroxide is not storable over extended periods of time. Hydrogen peroxide decomposes exothermically at a rate of 1–3% per year and can explode at temperatures above 448 K [15]. Hydrogen peroxide is therefore not deemed suitable for the exploration missions discussed in this paper which each have multi-year cruise phases, as shown in Table 3.

The performance of nitrous oxide (N_2O) and IRFNA is very similar but is low compared to the performance of the other oxidizers considered. Nitrous oxide has been used extensively for small-scale hybrid rocket test programs and is the oxidizer used in Spaceship 1 and 2 [31]. However, nitrous oxide does not have in-space heritage. Nitrous oxide also does not have high density, see Table 1. Thus, nitrous oxide is not considered as an oxidizer for these missions.

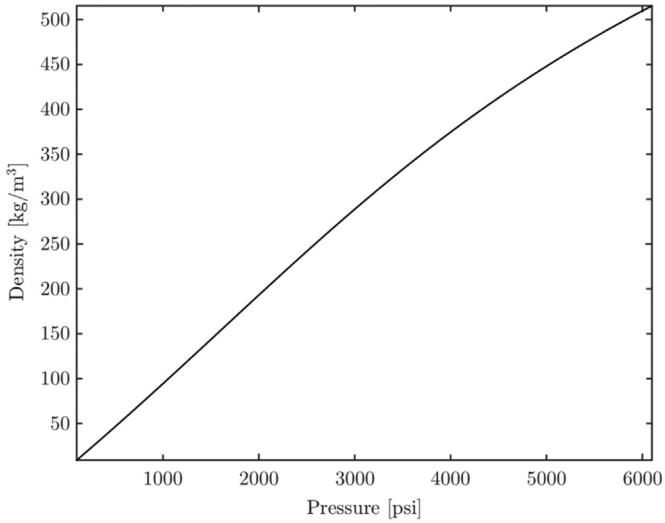

Fig. 6. Density of gaseous oxygen versus pressure at 293.15 K from Ref. [30].

IRFNA has been used in liquid bipropellant tactical missiles and has significant flight heritage from early in-space systems. One of the major benefits of IRFNA is its high density. The increased density of IRFNA might compensate for the lower performance of the oxidizer and thus it is considered as an oxidizer for the two missions.

MON-3 has reasonable performance and is a storable liquid oxidizer with significant heritage. A design utilizing MON-3 as an oxidizer is considered for the two missions.

Empirical regression rate data for the combustion of MON-3 with other hybrid rocket fuels is not published and thus has to be estimated. The regression rate of the fuel is a function of heat transfer to the fuel surface predominantly via turbulent diffusion. In the absence of further information, the regression rate of MON-3 with paraffin wax is thus approximated based on the flame temperature of a MON-3/paraffin flame as compared to the flame temperature of a nitrous oxide/paraffin flame and a gaseous oxygen/paraffin flame at ideal operating conditions for peak Isp_{VAC}. The adiabatic flame temperature for MON-3/paraffin, nitrous oxide/paraffin, and gaseous oxygen/paraffin were determined via CEA to be 3272 K, 3237 K, and 3459 K, respectively. The regression rate of MON-3 was therefore estimated using the regression rate parameters for nitrous oxide. This assumption is only approximate. Experimental testing is required in order to obtain an accurate regression rate estimate for this oxidizer. As described in the design section of this paper, the estimate of the regression rate parameters does not affect the calculations of propellant mass required to achieve a given ΔV, rather it effects the geometry of the fuel grain, the oxidizer mass flow rate required to achieve the design O/F and, therefore, also the estimated thrust of the motor. These values have only a secondary effect on the system mass, and so the masses presented using the approximated regression rate parameters are expected to be reasonable estimations of the final system mass. Other papers considering system studies for these vehicles, such as Reference [4], made similar assumptions in the absence of test data.

The n exponent for the combustion of IRFNA is taken from Table 7. It is assumed that this exponent remains the same for other hybrid fuels. For both IRFNA and MON-3, the value of a_o is scaled based on the selection of fuel and the relative burn rates of these fuels with other oxidizers. For designs using the addition of 30% aluminum powder, the value of a_o is scaled by a further 10% to account for the typically observed increase in regression rate of aluminized fuels over neat fuels.

Table 8
Comparison of hybrid propulsion system utilizing MON-3 oxidizer with a propulsion system utilizing IRFNA as the oxidizer.

Parameter	Units	MON-3	IRFNA	MON-3	IRFNA
Fuel	[-]	PE Wax	PE Wax	PE Wax + 30% Al	PE Wax + 30% Al
Pressurant	[-]	He	He	He	He
Hybrid ΔV	[m/s]	1520	1520	1520	1520
Hybrid Isp‡	[s]	322	307	326	314
Ideal Impulse Density	[s kg/L]	448	466	471	491
Burn Time	[s]	81	89	86	88
Thrust	[N]	34961	31696	33189	31929
Fuel Mass	[kg]	162	149	225	197
Oxidizer Mass	[kg]	758	807	684	741
Pressurant Mass	[kg]	5	5	4	4
Total Propellant Mass	[kg]	925	960	913	943
Primary Structure Mass	[kg]	79	75	75	72
Propellant Mass and Primary Structure Mass	[kg]	1004	1035	988	1015

‡ Isp assumes that combustion efficiency is 95% and nozzle efficiency is 99%.

The selection of oxidizer for these exploration missions is evaluated by comparing designs for IRFNA versus MON-3, see Table 8. It can be seen in this table that the masses for both of the systems is of the same order, however the MON-3 system is lighter. The greater performance of MON-3 has a larger effect on the primary propulsion mass than the larger density of IRFNA. MON-3 is also currently widely used for in-space liquid bipropellant systems and is therefore selected as the oxidizer of choice for the two missions analysed here.

The fuel used for both propulsion designs presented in Table 8 was PE Wax. With the exception of PMMA, the performance of all hydrocarbon fuels introduced in Table 5 is very similar when combusted with MON-3; see Fig. 7.

The selection of fuel has the greatest effect on the burn time of the hybrid rocket motor, and hence on the thrust of the motor, Table 9. Designs are shown in this table for each neat hydrocarbon fuel as well as for each fuel with 30% aluminum powder. Note that the higher ideal performance of the aluminized fuel grains may be challenging to realize in practice. Combustion of solid aluminum can lead to decreased combustion efficiency and issues with slag in the post combustion chamber. Paraffin fuel grains with the dimensions prescribed in Fig. 1 were not found to be suitable for the Europa mission as their fast burn rates led to vehicle accelerations larger than 29.4 m/s^2 (3 g) towards the end of the burn.

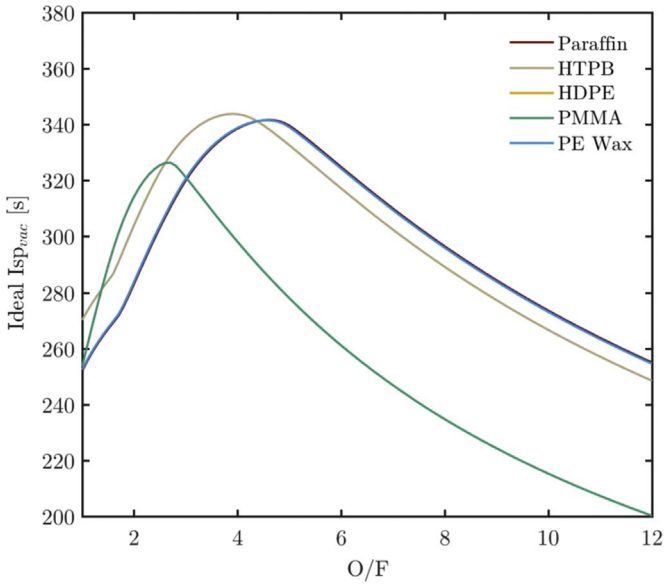

Fig. 7. Ideal Isp$_{VAC}$ versus *O*/*F* for a range of fuels with MON-3. This figure is generated using Chemical Equilibrium with Applications [12], with a nozzle area ratio of 100 and chamber pressure of 1.38 MPa (200 psi).

The classical fuels HTPB, HDPE and PMMA all satisfy the acceleration requirement and the slower burn rate of these fuels has the beneficial effect of reducing the nozzle throat diameter, and hence the nozzle mass. However, their slow burn rates require low oxidizer mass fluxes in order to achieve the design *O*/*F* ratio throughout the burn. The mass fluxes of the motors using classical fuels can be as low as 14 kg/m^{2}s by the end of the burn, and may lead to problems with motor operation, such as combustion instabilities and possible motor extinction. For this reason, PE wax with 30% aluminum powder is selected as the fuel of choice for a hybrid motor using a length-to-diameter ratio of 6 as suggested in Fig. 1. The faster burning paraffin wax fuel is only suitable if the length of the motor is reduced, this shall be discussed further in the context of packaging.

5.2. Chamber pressure and nozzle area ratio

The ideal combustion chamber pressure and nozzle area ratio for these motors cannot be determined independently. Increasing the nozzle area ratio monotonically increases the system performance, however it also results in a larger nozzle mass, volume, and length. Increasing the combustion chamber pressure also increases the system performance, and results in a smaller nozzle throat required for a given propellant flow rate, thereby reducing the size of the nozzle for a given nozzle area ratio. However, increasing the combustion chamber pressure can also increase the required structural mass since the combustion chamber and tanks must be designed for higher pressure operation. The net effect of changing the combustion chamber pressure and nozzle area ratio is shown in Fig. 8. The total system mass is minimized when a combustion chamber pressure of 2.07 MPa (300 psi) is used. As expected, increasing the nozzle area ratio increases the system performance, however, most of the gain associated with increasing the area ratio is obtained with an area ratio of 100. Any increase in area ratio above this value only marginally decreases the system mass, but results in a much larger nozzle length. Thus, a nozzle area ratio of 100 and a combustion chamber pressure of 2.07 MPa (300 psi) are selected for the final hybrid designs.

5.3. Packaging

One of the benefits of hybrid rocket motors is the flexibility in their packaging. No specific packaging requirements were given for the two missions analysed here. In reality, the selection of launch vehicle and the geometry of the spacecraft will impose volume and configuration constraints. The hybrid rocket motor designs analysed so far in this paper have assumed that one main motor is used. It is possible to design an alternative system utilizing multiple hybrid rocket motors operating in parallel, such as the propulsion system proposed in Reference [4]. Such a system could utilize differential throttling between the four motors for TVC during the main burn. This configuration was analysed for the Europa mission and found to increase the propulsion system mass by 5–10%, as compared to a single motor system and thus is not recommended as the configuration of choice for an orbit insertion motor unless required to meet the packaging constraints. In the absence of such constraints for the two missions presented here, a simple, single main hybrid rocket motor is used for the main burns, with heritage monopropellant thrusters used for ACS and TVC.

The fuel geometry constraints shown in Fig. 1 produce propulsion systems with a long, thin geometry compared to existing

Table 9
Comparison of hybrid propulsion systems utilizing various fuels. MON-3 is the assumed oxidizer for all of these systems.

Parameter	Units	Paraffin	HTPB	HDPE	PMMA	PE Wax	Paraffin +30% Al	HTPB +30% Al	HDPE +30% Al	PE Wax+30% Al	PMMA +30% Al
Hybrid Isp‡	[s]	322	324	322	308	322	327	329	326	326	315
O/F	[-]	4.7	4.0	4.6	2.7	4.6	3.0	2.5	3.0	3.0	1.7
Ideal Impulse Density	[s kg/L]	447	444	451	443	448	469	467	473	471	478
Burn Time	[s]	28	106	267	284	81	29	119	283	86	322
Thrust	[N]	102971	26716	10635	9891	34961	96693	24015	10059	33189	8780
Max. Acceleration	[m/s^2]	71	18	7	7	24	66	16	7	23	6
Min. Mass Flux	[kg/m^{2}s]	254	58	27	20	87	199	42	21	69	14
Propellant Mass	[kg]	925	920	925	956	925	913	908	913	913	937
Primary Dry Mass	[kg]	106	74	63	61	79	101	69	60	75	56
Total Mass†	[kg]	1030	994	988	1017	1004	1014	977	973	988	993

‡ Isp assumes that combustion efficiency is 95% and nozzle efficiency is 99%.
† Total mass in this table refers only to propellant mass and primary propulsion mass.

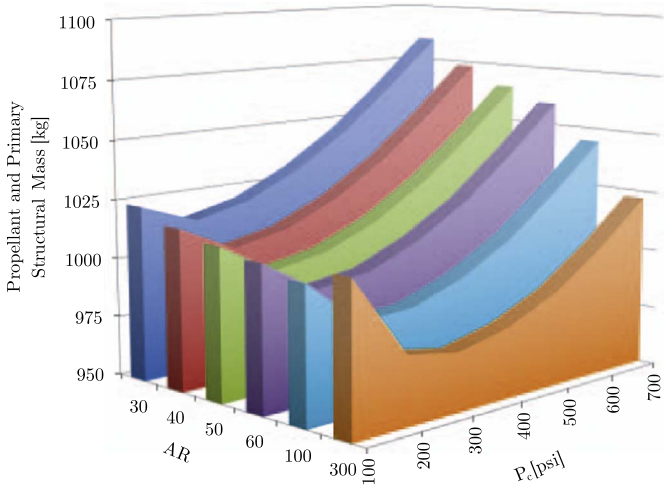

Fig. 8. Propellant and primary structural mass for a Europa flyby mission hybrid rocket motor versus nozzle Area Ratio (AR) and combustion chamber pressure (P_c). PE wax with 30% aluminum and MON-3 are used as the fuel and oxidizer of this system. The structural masses are calculated assuming COPV tanks and a titanium combustion chamber.

solid and liquid systems. Alternative geometries with smaller length-to-diameter ratios are explored in case the large propulsion system lengths prove prohibitive to their adoption.

Decreasing the length of the hybrid rocket fuel grain requires a shift to a faster burning fuel such as paraffin wax in order to operate at reasonable oxidizer mass fluxes without shifting to a complicated multi-port fuel grain design. The main parameters for these motors, as well as motors for Uranus are provided in Tables 10 and 11. Fig. 9 provides a scale comparison of the dimension of the two motor designs for the Europa mission. Note that the total system masses for both configurations are very similar and both propulsion systems satisfy the mission requirements for the Europa mission; however, the short motor for the Uranus mission does not meet the 3 g maximum acceleration requirement.

5.4. Comparison to baseline systems

The hybrid propulsion systems presented in the previous section are compared to the baseline propulsion systems. The baseline systems were discussed in detail in section II and section III. They are comprised of bipropellant liquid engines using NTO and hydrazine, and monopropellant hydrazine thrusters for TVC and ACS. The hybrid propulsion systems utilize the baseline thrusters for TVC and ACS. Secondary propulsion system masses are

Table 10
Comparison of a long and short hybrid propulsion system for the Europa flyby mission. MON-3 is the oxidizer for both systems.

Europa Parameter	Units	Long Motor	Short Motor
Fuel	[-]	PE Wax+30% Al	Paraffin+30% Al
Pressurant	[-]	He	He
Hybrid Isp‡	[s]	326	327
Burn Time	[s]	86	74
Thrust	[N]	33189	38373
Max Acceleration	[m/s^2]	23	26
Initial G_O	[kg/m^{2}s]	276	199
Final G_O	[kg/m^{2}s]	69	50
L/D_O	[-]	6	3
Nozzle and CC Length	[cm]	400	336
Fuel Mass	[kg]	225	225
Oxidizer Mass	[kg]	684	684
Pressurant Mass	[kg]	4	4
Total Propellant Mass	[kg]	913	913
Primary Structure Mass	[kg]	75	76
Propellant and Primary Structure Mass	[kg]	988	990

‡ Isp assumes that combustion efficiency is 95% and nozzle efficiency is 99%.

Table 11
Comparison of a long and short hybrid propulsion system for a mission to Uranus. MON-3 is the oxidizer for both systems.

Uranus Parameter	Units	Long Motor	Short Motor
Fuel	[-]	PE Wax + 30% Al	Paraffin + 30% Al
Pressurant	[-]	He	He
Hybrid Isp‡	[s]	326	327
Burn Time	[s]	103	89
Thrust	[N]	47646	55087
Max Acceleration	[m/s^2]	26	30
Initial G_O	[kg/m^{2}s]	276	199
Final G_O	[kg/m^{2}s]	69	50
L/D_O	[-]	6	3
Nozzle and CC Length	[cm]	479	403
Fuel Mass	[kg]	386	386
Oxidizer Mass	[kg]	1177	1177
Pressurant Mass	[kg]	8	8
Total Propellant Mass	[kg]	1571	1571
Primary Structure Mass	[kg]	132	135
Propellant and Primary Structure Mass	[kg]	1703	1706

‡ Isp assumes that combustion efficiency is 95% and nozzle efficiency is 99%.

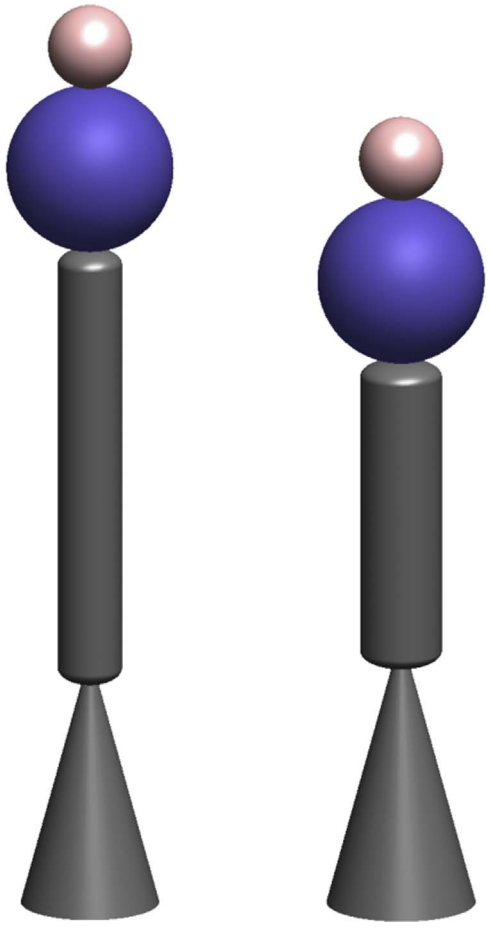

Fig. 9. Example configurations for a long (left) and short (right) hybrid rocket motor for the Europa mission. Oxidizer tanks are shown in blue, pressurant gas tanks in red, and the main motor in gray. Motor geometry is taken from the designs presented in Table 10.

Table 12
Comparison of the baseline and hybrid propulsion system for Europa flyby mission.

Europa				
Parameter	Units	Baseline	Hybrid- Baseline ΔV	Hybrid- ΔV With Less Gravity Loss
ΔV	[km/s]	1.52	1.52	1.37
Propellant for ΔV‡	[kg]	888	913	840
Propellant for TVC and ACS	[kg]	118	118	118
Total Propellant	[kg]	1005	1031	958
CBE Dry Mass	[kg]	175	222	214
CBE Wet Mass	[kg]	1180	1253	1173
Contingency*	[%]	10%	10%, 20% new development	10%, 20% new development
Wetmass with Contingency	[kg]	1198	1279	1198

‡ Includes residuals and pressurant gas.
* 10% contingency is applied to dry mass with flight heritage *e.g.* the tanks. 20% contingency is applied to dry mass requiring new development *e.g.* the combustion chamber.

calculated assuming the feedline masses for the hybrid system are equivalent to the baseline systems, given that both systems use the same oxidizer and both use hydrazine for TVC and ACS. Other secondary propulsion system masses such as the mass for mounts and bosses for the hybrid motor are calculated and added to the total propulsion system dry mass. The resulting system masses for the Europa and Uranus missions are provided in Tables 12 and 13.

Table 13
Comparison of the baseline and hybrid propulsion system for a mission to Uranus.

Uranus				
Parameter	Units	Baseline	Hybrid- Baseline ΔV	Hybrid- ΔV With Less Gravity Loss
ΔV	[km/s]	1.96	1.96	1.76
Propellant for ΔV‡	[kg]	1445	1571	1454
Propellant for TVC and ACS	[kg]	139	139	139
Total Propellant	[kg]	1585	1710	1593
CBE Dry Mass	[kg]	114	199	188
CBE Wet Mass	[kg]	1699	1909	1781
Contingency‡	[%]	10%	10%, 20% new development	10%, 20% new development
Wetmass with Contingency	[kg]	1710	1936	1806

‡ Includes residuals and pressurant gas.
* 10% contingency is applied to dry mass with flight heritage *e.g.* the tanks. 20% contingency is applied to dry mass requiring new development *e.g.* the combustion chamber.

Note that the values listed in these tables use a long hybrid rocket motor configuration.

Two sets of hybrid rocket motor sizes are provided in Tables 12 and 13, the first ignores the increased thrust level of the hybrid rocket motor, which will act to decrease gravity losses during the orbit insertion burn. Gravity losses can account for approximately 10% of the required ΔV for an orbit insertion burn like the ones considered in this paper, see Reference [32]. The baseline propulsion systems for Europa and Uranus have thrust levels of only 458 N and 645 N, respectively. The use of a hybrid rocket motor has thrust approximately two orders of magnitude higher than this, resulting in a burn time two orders of magnitude shorter, which will almost totally remove the gravity losses. The second set of values in the table therefore assumes a 10% reduction in ΔV as a result of using the high-thrust propulsion system.

From Tables 12 and 13 we see that the hybrid propulsion system has comparable mass to the baseline bipropellant system for the Europa mission, but is not competitive with the current formulation for the Uranus mission. We believe that this is primarily because the assumptions used in the Uranus propulsion system baseline design were overly aggressive. A more detailed and realistic design of the baseline Uranus propulsion system is required to accurately compare the performance of the hybrid to existing in-space propulsion systems.

6. Areas for further investigation

There are a number of issues that require further investigation before any of the systems presented in this paper can be adopted. Foremost of these is the need to instigate a test program to investigate the relevant empirical regression rate values of a and n (see Eqs. 4 and 6) for the propellant combinations discussed here. All new propulsion systems typically require a full test program in order to both verify the design and resolve any issues with combustion instabilities.

The reduction in required ΔV for each mission resulting from using the high-thrust hybrid propulsion system also needs to be verified via a detailed trajectory analysis.

The ignition system for these motors was not described in this paper. It is hoped that a small igniter capable of multiple ignitions might be available for these systems, however this possibility has not been thoroughly investigated. If such an igniter is not available, then the authors believe that multiple small pyrotechnic devices with blow-out plugs may suffice for ignition if the number

of required ignitions is known *a priori* and is not too large. The proposed test program will need to thoroughly test the ignition scheme and verify that it will work in a near-vacuum environment.

The selection of an ignition system for this motor also raises the question of the power requirements of the propulsion system. These need to be quantified and compared to the power resources expected to be available on these spacecraft. It is expected that the hybrid propulsion system, which requires power for valve actuation, ignition and potentially some small amount for propellant tank heating, will have power requirements that are significantly less than those of the baseline bi-propellant system, which requires significant power to heat the hydrazine tank.

The issue of spacecraft control is briefly discussed in this paper under the context of overall system configuration. This area warrants a more detailed investigation, particularly in regards to control of the spacecraft during the main burn. Thrust misalignment, and its potential effect on the trajectory and attitude of the spacecraft, is also not examined in this work. Future work will need to investigate how control authority will be maintained throughout the main burn to determine whether the current thrust vector control system is sufficient or whether the thrust of the TVC thrusters will need to be increased.

Erosion of the nozzle throat during operation of the main motor is not considered in this study. Future work should evaluate the effect of nozzle erosion on the predicted motor performance and mass estimates presented in this paper. It is recommended that the effect of nozzle erosion is calculated using the approach described in Reference [22] where it is assumed that throughout the burn the nozzle undergoes erosion according to Eq. 14.

$$\dot{r}_n = a_n \frac{C_D}{c^* \eta} P_{n,ref} \tag{14}$$

The packaging of the propulsion system was discussed in this paper with alternative motor designs presented to demonstrate the flexibility of the hybrid rocket motor configuration. Future work should seek to gain more specific information on sizing constraints for these vehicles in order to finalize the design of a motor for these missions.

7. Conclusions

Feasible hybrid propulsion systems have been designed for two exploration missions. The propulsion systems are each comprised of a single main hybrid rocket motor using aluminized Poly-Ethylene (PE) wax and MON-3, and a monopropellant ACS and TVC system using hydrazine. The proposed systems are capable of meeting the mission requirements. The proposed system has very similar performance to the baseline bipropellant propulsion system for the Europa flyby mission and is expected to significantly reduce the propulsion system cost and power requirements. Experimental testing is deemed necessary to advance the design and verify the predicted performance.

Acknowledgments

The authors would like to acknowledge the Jet Propulsion Laboratory's Strategic University Research Partnership program for financial support of the. E. Jens would also like to acknowledge the support of Zonta International in the Form of the Amelia Earhart Fellowship. Heartfelt thanks also go to Barry Nakazono for his advice.

References

[1] A.A. Chandler, et al., Hybrid propulsion in-situ resource utilization test facility development, in: 50th AIAA/ASME/SAE/ASEE Joint Propulsion Conference, American Institute of Aeronautics and Astronautics, 2014.
[2] A.C. Karp, et al., Hybrid propulsion in-situ resource utilization test facility results, in 51st AIAA/SAE/ASEE Joint Propulsion Conference. 2015, American Institute of Aeronautics and Astronautics.
[3] A.A. Chandler, et al., A two-stage, single port hybrid propulsion system for a mars ascent vehicle, in: 46th AIAA/ASME/SAE/ASEE Joint Propulsion Conference & Exhibit, American Institute of Aeronautics and Astronautics, 2010.
[4] A.A. Chandler, B.J. Cantwell, G.S. Hubbard, Hybrid propulsion for solar system exploration, in: 47th AIAA/ASME/SAE/ASEE Joint Propulsion Conference & Exhibit, American Institute of Aeronautics and Astronautics, 2011.
[5] A.J. Boiron, B.J. Cantwell, Hybrid rocket propulsion and in-situ propellant production for future mars missions, in: 49th AIAA/ASME/SAE/ASEE Joint Propulsion Conference, American Institute of Aeronautics and Astronautics, 2013.
[6] Jens, E., et al., Hybrid CubeSat Propulsion System with Application to a Mars Aerocapture Demonstration Mission, in: Proceedings of the 65th International Astronautical Congress, International Astronautical Federation Toronto, Canada, Toronto, Canada, September 2014.
[7] Space Studies Board, Vision and Voyages for Planetary Science in the Decade 2013-2022, National Academies Press, 2011.
[8] D. Brown, et al., All Systems Go for NASA's Mission to Jupiter Moon Europa, National Aeronautics and Space Administration: NASA Headquarters, Washington, 2015.
[9] Europa Study Team, Europa Study 2012 Report, National Aeronautics and Space Administration, 2012.
[10] S. Saikia, et al., MUSEings on Uranus: Exploration of the Ice-Giant, LPI Contrib. 1795 (2014) 8074.
[11] J. Spencer, C. Nieber, Mission Concept Study: Titan Saturn System Mission, National Aeronautics and Space Administration, 2010, Planetary Science Decadel Survey.
[12] B. McBride, S. Gordon, Computer program for complex chemical equilibrium compositions and applications, in: L.R. Center (Ed.), National Aeronautics and Space Administration Cleveland, Ohio,1996.
[13] A.C. Wright, USAF Propellant Handbooks. Nitric Acid/Nitrogen Tetroxide Oxidizers. Vol. II., DTIC Document, 1977.
[14] R.W. Humble, G.N. Henry, W.J. Larson, Space Propulsion Analysis and Design, McGraw-Hill, New York, 1995.
[15] G.P. Sutton, O. Biblarz, Rocket Propulsion Elements, John Wiley & Sons, 2010.
[16] E.W. Lemmon, M.L. Huber, M.O. McLinden, NIST Reference Fluid Thermodynamic and Transport Properties–REFPROP,Version, 2002.
[17] M.J. Chiaverini, Hybrid propulsion, Encycl. Aerosp. Eng. (2010).
[18] D. Cruise, Theoretical Computations of Equilibrium Compositions, Thermodynamic Properties, and Performance Characteristics of Propellant Systems. DTIC.
[19] G. Zilliac, M.A. Karabeyoglu, Hybrid rocket fuel regression rate data and modeling, AIAA Paper 2006, p. 4504.
[20] M.O. Chemical, Product Data Sheet: Marcus Low Molecular Weight Polyethylene Homopolymers 2000 [cited 2015; Typical Properties Marcus Polyethylene Homopolymer Waxes]. Available from: ⟨http://www.marcusoil.com/pdf/PRD-HOMpublisher_n.pdf⟩.
[21] A.M. Karabeyoglu, B.J. Cantwell, J. Stevens, Evaluation of the homologous series of normal alkanes as hybrid rocket fuels, in: 41st AIAA/ASME/SAE/ASEE Joint Propulsion Conference & Exhibit, American Institute of Aeronautics and Astronautics, 2005.
[22] E. Toson, A.M. Karabeyoglu, Design and optimization of hybrid propulsion systems for in-space application, in: 51st AIAA/SAE/ASEE Joint Propulsion Conference, American Institute of Aeronautics and Astronautics, 2015.
[23] G. Zilliac, et al. Peregrine hybrid rocket motor development. 50th AIAA/ASME/SAE/ASEE Joint Propulsion Conference, American Institute of Aeronautics and Astronautics, Propulsion and Energy Forum, 2014.
[24] B. Evans, et al., Hybrid Rocket Investigations at Penn State university's High Pressure Combustion Laboratory: Overview and Recent Results, AIAA Paper 2009, p. 2009.
[25] P. George, et al., Fuel regression rate in hydroxyl-terminated-polybutadiene/gaseous-oxygen hybrid rocket motors, J. Propuls. Power 17 (1) (2001) 35–42.
[26] A.M. Karabeyoglu, Lecture 10 – Hybrid Rocket Propulsion Design Issues, Stanford University, 2011, AA284a Advanced Rocket Propulsion course.
[27] E. Doran, et al., Nitrous oxide hybrid rocket motor fuel regression rate characterization, AIAA 5352 (2007).
[28] R. Muzzy, Applied hybrid combustion theory, in: AIAA/SAE Eighth Joint Propulsion Specialist Conference, New Orleans, LA, 1972.
[29] L. Simurda, G. Zilliac, Continued testing of the high performance hybrid propulsion system for small satellites, in: 51st AIAA/SAE/ASEE Joint Propulsion Conference, 2015.
[30] E.W. Lemmon, M.O. McLinden, D.G. Friend, Thermophysical Properties of Fluid Systems, in NIST Chemistry WebBook, in: P.J. Linstrom, W.G. Mallard, (Ed.)., National Institute of Standards and Technology: Gaithersburg MD.
[31] E. Seedhouse, SpaceShipTwo: VSS Enterprise, Springer International Publishing 2015, pp. 65–85, in Virgin Galactic.
[32] T.H. Sweetser, et al., Trajectory design for a Europa orbiter mission: a plethora of astrodynamic challenges, Adv. Astronaut. Sci. 95 (1997) 901–920.